Supporting Information for

The Deep Permafrost Carbon Pool of the Yedoma Region in Siberia and Alaska

By Jens Strauss[1], Lutz Schirrmeister[1], Guido Grosse[2,1], Sebastian Wetterich[1], Mathias Ulrich[3], Ulrike Herzschuh[1], Hans-Wolfgang Hubberten[1]

([1]Alfred Wegener Institute Helmholtz Centre for Polar and Marine Research, Periglacial Research Unit, Potsdam, Germany; [2]Geophysical Institute, University of Alaska Fairbanks, Fairbanks, USA; [3]Institute for Geography, Leipzig University, Germany)
Geophysical Research Letters, 2013

Content

1. Terminology and Methods

1.1 Terminology and Abbreviations

1.1.1 Terminology

Segregated ice: Ice in discrete layers (bands) or ice lenses (not in wedge ice), formed by freezing of water within the sediments (e.g. Fig. 2d; according to *van Everdingen* [1998, revised 2005]).

Thaw-lake basin (drained): = thermokarst depression (Fig. 2b). Drained thaw-lake basins are the result of degradation of Yedoma deposits by lake formation. The Russian literature also describes a drained thaw-lake basin as an *"alas"*, defined as a large depression of the ground surface produced when a large area of thick and exceedingly ice-rich permafrost thaws (according to *van Everdingen* [1998, revised 2005]).

Thermokarst (process): A process by which characteristic landforms, like basins caused by surface subsidence, result from the thawing of ice-rich permafrost (according to *van Everdingen* [1998, revised 2005]).

Thermokarst deposits: Used in this study to describe the frozen deposits accumulated in drained thaw-lake basins and thermo-erosional valleys.

Wedge ice: A massive, generally wedge-shaped ice body, composed of foliated or vertically banded ice (Fig. 2a; according to *van Everdingen* [1998, revised 2005]).

Yedoma: A suite of late Pleistocene ice- and organic-rich silty sediments that accumulated in Beringia (unglaciated Siberia and Alaska) [*Schirrmeister et al.*, 2013].

Yedoma deposits: Used in this study to emphasize that the deposit itself (not the geomorphic or the stratigraphic position [*Schirrmeister et al.*, 2013]) is meant. The studied recent Yedoma deposits are undisturbed and unaltered by thermokarst processes (Fig. 2a,b).

Yedoma region: We used this term to outline the potential area for Yedoma deposit distribution, not to indicate the area where Yedoma deposits indeed occur (Fig. 1). The Yedoma region also includes thermokarst areas.

1.1.2 Important Abbreviations

BD: Bulk density in 10^3 kg/m^3 = g/cm^3

CH_4: Methane

CO_2: Carbon dioxide

Gt: gigatonne; 1 gigatonne = 10^9 tonnes = 10^{12}kg = 10^{15}g (= petagram; Pg)

OC: organic carbon

RCP: Representative Concentration Pathways

SEI: Segregated ice

SEIV: Segregated-ice volume

SI: Supporting information

TOC: Total organic carbon

WI: Wedge ice

WIV: Wedge-ice volume

1.2 Total Organic Carbon (TOC) Measurement

Before measurement of TOC, the samples were dried, homogenized, and milled using a ball mill (Fritsch pulverisette 5). Carbonate was removed by adding hydrochloric acid (4%). The sediment samples were measured twice with a carbon-nitrogen-sulphur analyzer (Elementar Vario EL III) or a TOC analyzer (Elementar Vario Max C; a device with integrated inorganic carbon removal). In each series of measurements, a blank capsule was used for background and several capsules of standards (Sulphanilamid, EDTA 10:40, IVA 2150, PACS 1, L-Glutamine, L-Cysteine) were determined with a device-specific accuracy of 0.1wt%.

1.3 Calculation of the Bulk Density, Segregated Ice, and Organic Carbon Density

For BD and SEI calculation samples were weighed in wet and oven-dry state during field expeditions. If no data for the density of the solid fraction (sediment density, ρ_s, 10^3 kg/m³) was available, we assumed that ρ_s for BD calculation is equal to the density of its dominant component, quartz (2.65 10^3 kg/m³). Instead of using quartz density, the sediment density of a subset of samples (202) was determined using a helium gas displacement pycnometer (AccuPyc-1330, Micromeritics) for validation. To determine BD (10^3 kg/m³), the volume of the solids (V_s, 10^{-6} m³) was derived first. The mass of solid particles (m_s) and the solid fraction density (ρ_s) are used in equation (S1):

$$V_s = \frac{m_s}{\rho_s} \quad \text{(S1)}$$

After that, the porosity (ϕ) was calculated (equation (S2)) using pore volume (V_p, 10^{-6} m³):

$$\phi = \frac{V_p}{V_p + V_s} \quad \text{(S2)}$$

It is appropriate to assume that pores in frozen deposits are ice-saturated if the SEI is >20wt% [*Strauss et al.*, 2012]. With this assumption, the SEI gives an estimation of the pore volume.

For determining ice volume an ice density of 0.91 10^3 kg/m³ was assumed. BD was then calculated using its inverse relationship with porosity (equation (1)).

For error estimation, we compared measured and calculated BD for a subgroup of the samples (Fig. S2). To assess a mean, the difference between measured and calculated samples is 12% for both Yedoma (n=90) and thermokarst (n=36) deposits.

To calculate the OC density, the BD calculations and measurements were combined with TOC values and WIV. The volumetric OC calculation (OC density, kg/m³) was performed according to:

$$\text{OC density (kg/m}^3\text{)} = \text{BD } (10^3\text{kg /m}^3) \times \frac{100 - \text{WIV}}{100} \times \frac{\text{TOC}}{100} \times 1{,}000 \quad \text{(S3)}$$

1.4 Calculation of the Wedge-Ice Volume (WIV)

1.4.1 Assumptions and Calculation

WIV estimation is based on the simplification that polygons are squares. This approach does not account for active-layer thickness, and WIV calculations are only done for layers containing WI. In Fig. S1 the variables are sketched and defined.

For epigenetic ice wedges it is assumed that a frontal cut of an ice wedge has a shape of an isosceles triangle (Fig. S1, right side). The variables used to calculate epigenetic WIV are defined as: VoP: volume of the polygonal block (cuboid with a squared top), with VoP= $A^2 \times H$; A: polygon size, and H: polygon height; VoS: volume of sediment block (truncated pyramid), with VoS = ⅓ × H × (A^2+AB+B^2) and A: polygon size (=base side length), B: surface polygon length (top side length): B = A-C; C: maximum epigenetic ice-wedge width. This approach enables us to calculate the epigenetic WIV using the volume of a truncated pyramid to represent the sediment block framed by ice wedges [*Kanevskiy et al.*, 2013]. The WIV is calculated according to equation (S4):

$$\text{WIV}_{\text{epigenetic}} = \frac{\text{VoP} - \text{VoS}}{\text{VoP}} \Leftrightarrow 1 - \frac{H \times (A^2 + AB + B^2)}{H \times 3A^2} \Leftrightarrow 1 - \frac{A^2 + A \times (A - C) + (A - C)^2}{3A^2} \quad \text{(S4)}$$

This approach after *Kanevskiy et al.* [2013] is only feasible for epigenetic wedges, which occur mostly in the studied thaw lake basin thermokarst deposits. For syngenetic Yedoma deposit ice wedges, we deduced equation (S5), assuming that a frontal cut of this ice wedge type is rectangular in shape (Fig. S1, left side). Yedoma deposit VoS is assumed to be VoS = H × $(A-D)^2$. Hence, we used a different equation (S5) for syngenetic WIV calculation:

$$\text{WIV}_{\text{syngenetic}} = \frac{\text{VoP} - \text{VoS}}{\text{VoP}} \Leftrightarrow 1 - \frac{H \times (A - D)^2}{H \times A^2} \Leftrightarrow 1 - \frac{A^2}{A^2} - \frac{2AD + D^2}{A^2} \Leftrightarrow \frac{2AD - D^2}{A^2} \quad \text{(S5)}$$

D: mean (with depth) width of a syngenetic ice wedge. All other variables are similar to those used in the calculation of $WIV_{epigenetic}$.

1.4.2 Measuring Required Parameters for Wedge-Ice Volume Calculation

Wedge Ice Width

WI width is based on field measurements extracted from the literature [*Meyer et al.*, 2002a,b; *Grigoriev et al.*, 2003; *Magens*, 2005; *Boike et al.*, 2008; *Wetterich et al.*, 2008; *Hoffmann*, 2011; *Kanevskiy et al.*, 2011, 2012, 2013; *Opel et al.*, 2011; *Boereboom et al.*, 2013]. Forty-four measured Yedoma ice wedges at 14 sites were identified. The sites were merged to 10 regions/sites (Cape Mamontov Klyk, Lena Delta, Bykovsky Peninsula, Muostakh Island, New Siberian Islands, Dmitry-Laptev Strait, Duvanny Yar, Alaskan North Slope, Beaufort Sea coast, and interior Alaska) and each region was assigned a mean WI width. To determine thermokarst deposit WI width, 40 measured ice wedges were used from 16 sites, grouped into 6 regions/sites (Cape Mamontov Klyk, Lena Delta, Bykovsky Peninsula, Tiksi area, New Siberian Islands, and Dmitry-Laptev Strait) with a mean value shown in Tab. S4.

Polygon Size

The mean Yedoma and thermokarst deposit polygon sizes were determined by mapping very-high-resolution satellite imagery for four study sites: Cape Mamontov Klyk (1; numbers according to Fig. 1), Bykovsky Peninsula (5), Buor Khaya Peninsula (7), and Bol'shoy Lyakhovsky Island (13). For thermokarst deposits, the polygon mapping and size calculation were done according to *Ulrich et al.* [2011]. Polygons were digitized manually within ArcGIS™ using very-high-resolution GeoEye and Kompsat-2 satellite data (Fig. S3). Only if polygons were completely enclosed by rims or troughs, and the individual polygon form could be identified precisely, were they considered in the datasets. Clearly-recognizable fissures and troughs were mapped along their centerlines. The size was calculated as equivalent to the diameter of the polygon area [*Ulrich et al.*, 2011].

Since Yedoma deposits are often covered with thin Holocene deposits, their polygonal pattern is usually obscured. However, along thermokarst or thermo-erosion features, Yedoma polygonal patterns are exposed in the form of thermokarst mounds that represent erosional remnants of the former polygon centers. Yedoma deposit polygon sizes were therefore determined by measuring the distance between adjacent thermokarst-mound centers using a line feature class in ArcGIS™ (Fig. S3, right side) or with measuring tape in the field (Fig. S4c). Only the distances from one individual mound center to each neighboring and clearly identifiable mound center were measured. Field measurements were done in 2002 on the

Bykovsky Peninsula (5; according to Fig. 1), Bel'kovsky Island (9), Kotel'ny Island (10), and Maly Lyakhovsky Island (12) study sites (Fig. S4c).

1.5 Calculation of Yedoma Region Coverage

We based our calculations on the extent of the Yedoma region as delineated in general maps of the potential Yedoma deposit area in Siberia [*Romanovskii*, 1993] and in maps showing ice-rich silt deposits we identified as the potential Yedoma deposit area in Alaska [*Jorgenson et al.*, 2008], resulting in a total coverage of 1,387,000 km². In detail we assume the Yedoma area as 1,141,000 km² for Siberia, 181,000 km² for Alaska and ~65,000 km² for regions with smaller known Yedoma deposit occurrences (e.g. south of Taymyr Peninsula, Chukotka, and Yukon Territory).

Based on literature data [*Grosse et al.*, 2005, 2006, 2013b; *Veremeeva and Gubin*, 2009; *Morgenstern et al.*, 2011; *Arcos*, 2012; *Jones et al.*, 2012; *Morgenstern*, 2012] (Tab. S7) the average of Yedoma deposit areas versus areas affected by degradation in several North Siberian sites was estimated, suggesting that 70% of the Yedoma region is affected by degradation or erosion. This results in an updated coverage for remaining Yedoma deposits of 416,000 km², in addition to about 971,000 km² covered by non-Yedoma deposits. To estimate the coverage of frozen thermokarst deposits in this non-Yedoma deposit fraction, we subtracted the thermokarst lake area (considered to represent unfrozen deposits; 150,000 km², extracted for the Yedoma region from *Grosse et al.* [2013a] (lakes >0.1 km²) corrected with additional "missing" lake area (up to 80%) [*Grosse et al.*, 2008] and other literature data [*Grosse et al.*, 2005, 2006, 2013b; *Veremeeva and Gubin*, 2009; *Morgenstern et al.*, 2011; *Arcos*, 2012; *Jones et al.*, 2012; *Morgenstern*, 2012] (Tab. S7) and the area of river deltas (Olenyok, Lena, Yana, Indigirka, Kolyma) of 47,000 km² in the Yedoma region [*Walker*, 1998]. The rivers, including fluvial and alluvial unfrozen sediments, are also excluded from consideration. The Alaskan deltas (Yukon and Colville) were already excluded in the map that we used [*Jorgenson et al.*, 2008]. Hence, we inferred that frozen thermokarst deposits cover approximately 775,000 km².

1.6 Calculation of the Yedoma Region Atmospheric CO_2 contribution

For a rough calculation of the potentially outgassing Yedoma region CO_2, we used the equation S6. According to Battle et al. [2000], the release of one Gt of carbon to the atmosphere increases the amount of CO_2 by 0.471 ppm. The amount of CO_2, if 20% of the

Yedoma region OC pool (20% of 211+160/-153 Gt; min: 11.6 Gt, mean: 42.2 Gt, max: 74.2 Gt) is emitted to the atmosphere, is calculated with equation (S6):

$$CO_2\ (ppm) = \frac{C \cdot 0.471}{2} \quad \text{(S6)}$$

The factor of ½ is the airborne effect, assuming that half of the CO_2 rise will be incorporated into the ocean and plant biomass.

1.7 Mean-Bootstrapping Technique to Calculate Organic Carbon Budgets

This bootstrapping technique is used because of a non-normal distribution of the parameters (Fig. 3 and S5) and for the calculation of non-parametric uncertainty estimates. Besides the observation-based bootstrapping, we additionally performed the calculation (5.000 repetitions) based on means for each variable with observations available (TOC, BD, WIV, thickness). We used sampling with replacement, which means that after we randomly draw an observation from the original sample we put it back before drawing the next observation. We calculated the Yedoma deposit frozen OC pool as 14±2 kg/m³ and thermokarst deposits as 55±13 kg/m³. WIV is included in this calculation. Separate from wedge ice, the Yedoma deposit frozen OC pool contain 26±4 kg/m³ and thermokarst deposits 60±14 kg/m³. Adding the total stored Yedoma deposit OC, 111±17 Gt**,** and the frozen thermokarst deposit OC, 237±57 Gt, the total frozen Yedoma region contains 348±73 Gt. The median of the obtained distributions for Yedoma deposit and thermokarst deposit OC budgets, 110 and 232 Gt respectively. However, inferred 16^{th} and 84^{th} percentiles (Yedoma: 95 Gt, 128 Gt; thermokarst: 181 Gt, 232 Gt) are markedly smaller compared to the observation-based bootstrapping because using single value estimates such as mean reduces the variability of the obtained distribution. Sensitivity analyses were conducted by running the OC budget calculation repeatedly; each calculation utilized the uncertainty of a single variable, i.e. by using the mean of all values in the calculation rather than a randomly sampled mean (SI, Tab. S8).

1.8 Inventory Calculation Based on Simple-Mean Values

To estimate an OC inventory based on our parameter dataset that is comparable to previous studies (e.g. *Zimov et al.* [2006]) using the arithmetic mean and assuming normal-distribution, our Yedoma region OC estimate results in 112 Gt for Yedoma deposits and 240 Gt for thermokarst deposits. The total Yedoma region pool using mean values is 352 Gt.

Hence, the Yedoma deposit frozen OC pool contains 14 kg/m³ and thermokarst deposits as 56 kg/m³. WIV is included in this calculation. Separate from wedge ice the Yedoma deposit frozen OC pool contain 27 kg/m³ and thermokarst deposits 60 kg/m³ if WIV is not included. Details with error estimates are shown in Table S1. Nonetheless because of data heterogeneity and non-normal distributions (Fig. 3, S5), we assume that applied bootstrapping statistics for OC budget calculation yields more realistic values.

2. Supporting Figures

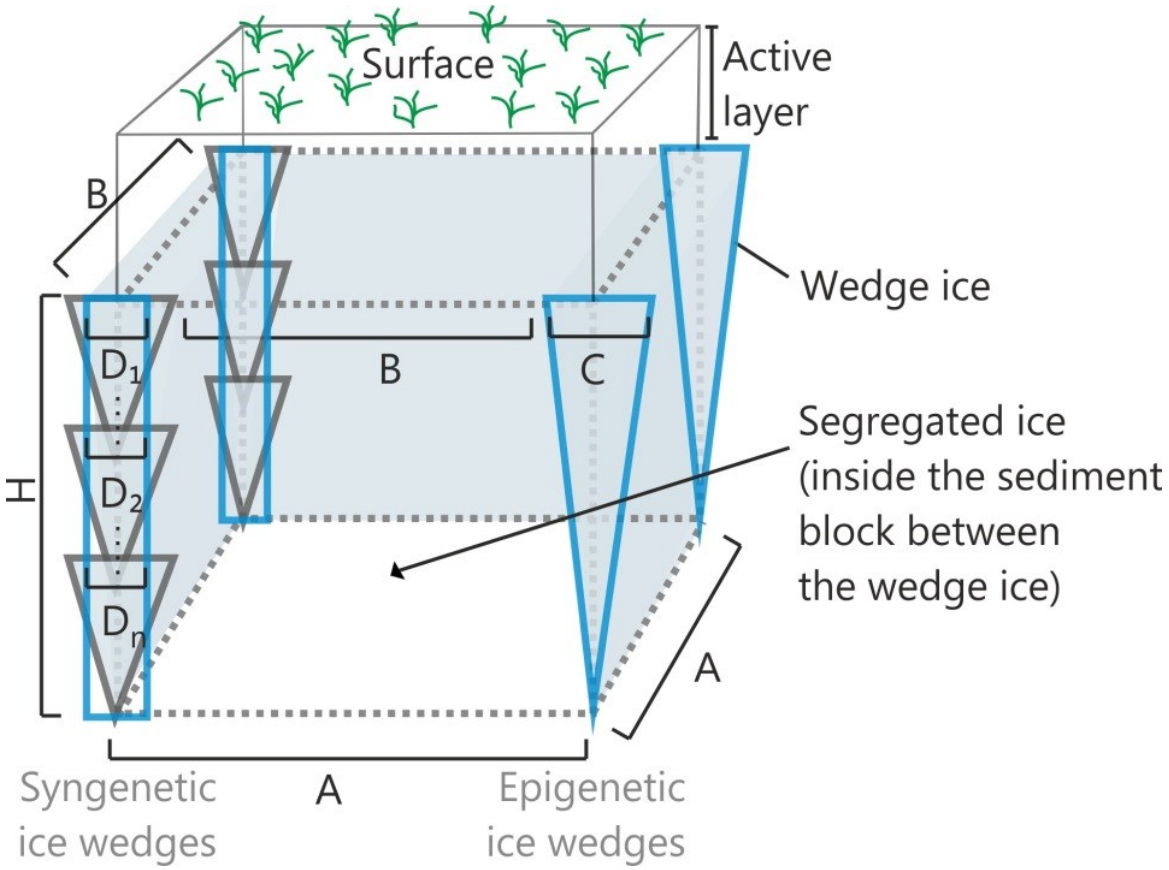

Figure S1. Idealized polygon scheme demonstrating variables used for wedge-ice volume (WIV) calculation. A: polygon size; B: surface polygon length; C: maximum width of epigenetic ice wedge; D: mean width of syngenetic ice wedge; H: polygon height. The equations for WIV calculation, (S4) and (S5), are described in SI, 1.4.1.

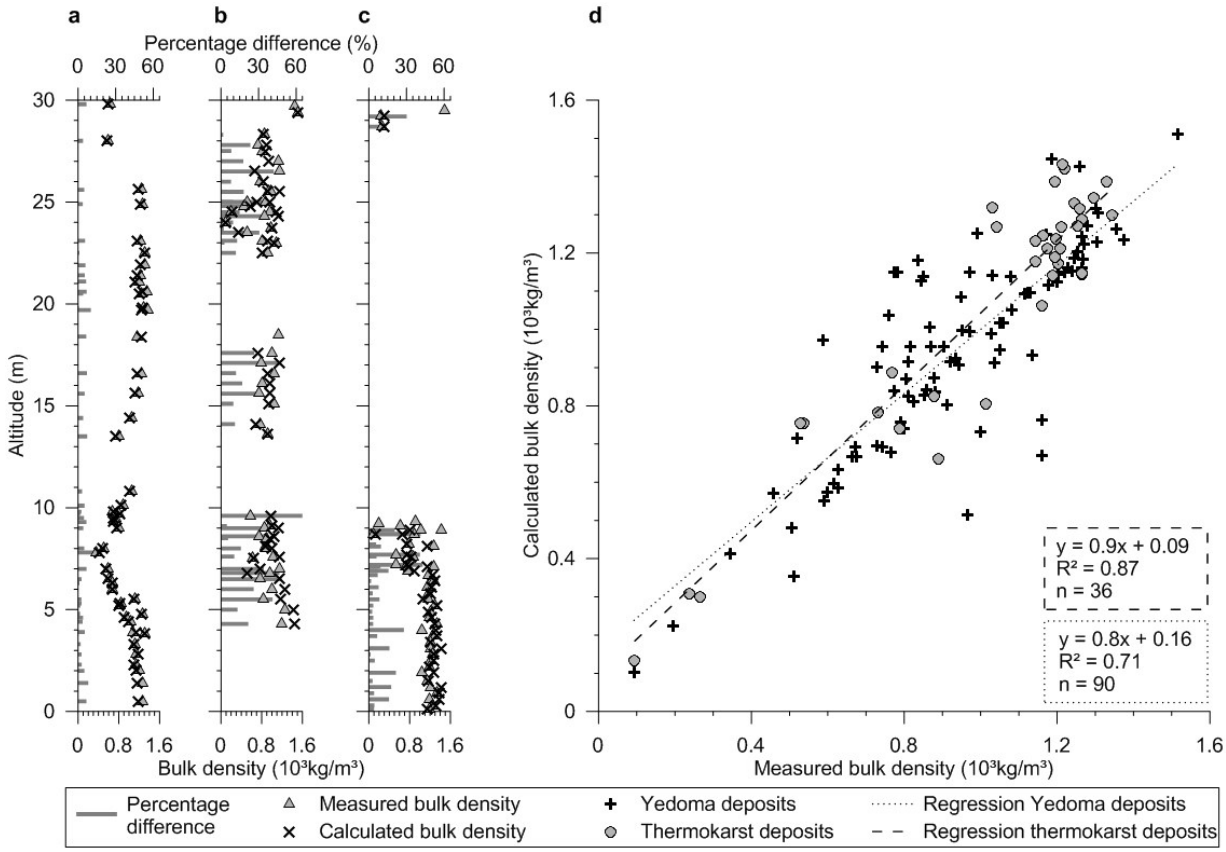

Figure S2. Measured and modeled bulk density (BD) data and error estimates. (a) Yedoma deposit exposure at Itkillik River, Alaska; (b) Yedoma deposit exposure at Buor Khaya, Laptev Sea, Siberia; (c) thermokarst deposits from Buor Khaya, Laptev Sea, Siberia; (d) relationship between measured and calculated BD of Yedoma and thermokarst deposits.

Fig. S2 shows the error estimates for our BD calculation in comparison with measured data. For this figure we only used samples for which both measurement and calculation were performed. The samples shown in Fig. S2a were measured during a winter expedition to the Itkillik River exposure (Fig. 1). The temperature in the field laboratory was below 0°C; therefore, it was possible to keep the sample frozen, ideal conditions for pumping a vacuum and measuring the displacement. The samples shown in Fig. S2b and c were collected and measured during the summer on the Buor Khaya Peninsula (Fig. 1), and it was not possible to generate a perfect vacuum without drawing in thawed material. As a result, the BD differences for these two sites (Fig. S2b, c) are higher than for the first site (Fig. S2a). Fig. S2d plots both measured and calculated BD for all sites and deposit types and indicates a good agreement between measured and calculated BD, with $R^2 = 0.71$ for Yedoma and $R^2 = 0.87$ for thermokarst deposits.

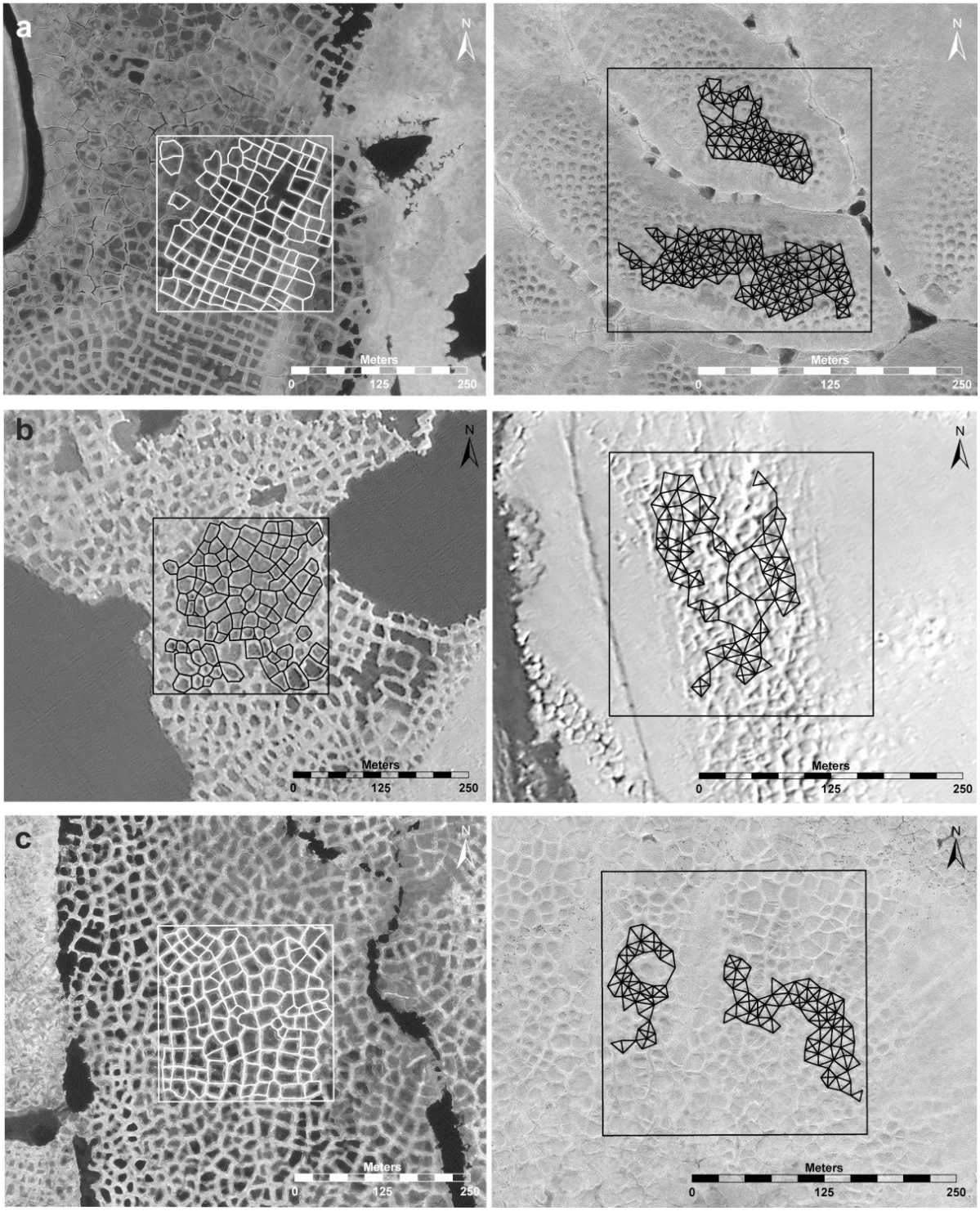

Figure S3. Methods used to measure polygon size. The satellite-image subsets illustrate polygon mapping for thermokarst deposits (left side) and distance measurements of thermokarst mounds for Yedoma deposits (right side) within a predefined area (box size) of 250 m × 250 m. (a) Cape Mamontov Klyk, site 1 in Fig. 1 (Geoeye, Band 4, 01.08.2010); (b) Bykovsky Peninsula, site 5 in Fig. 1 (Kompsat 2; Band 4, 26.08.2010); and (c) Buor Khaya Peninsula, site 7 in Fig. 1 (Geoeye, Band 4, 13.07.2009).

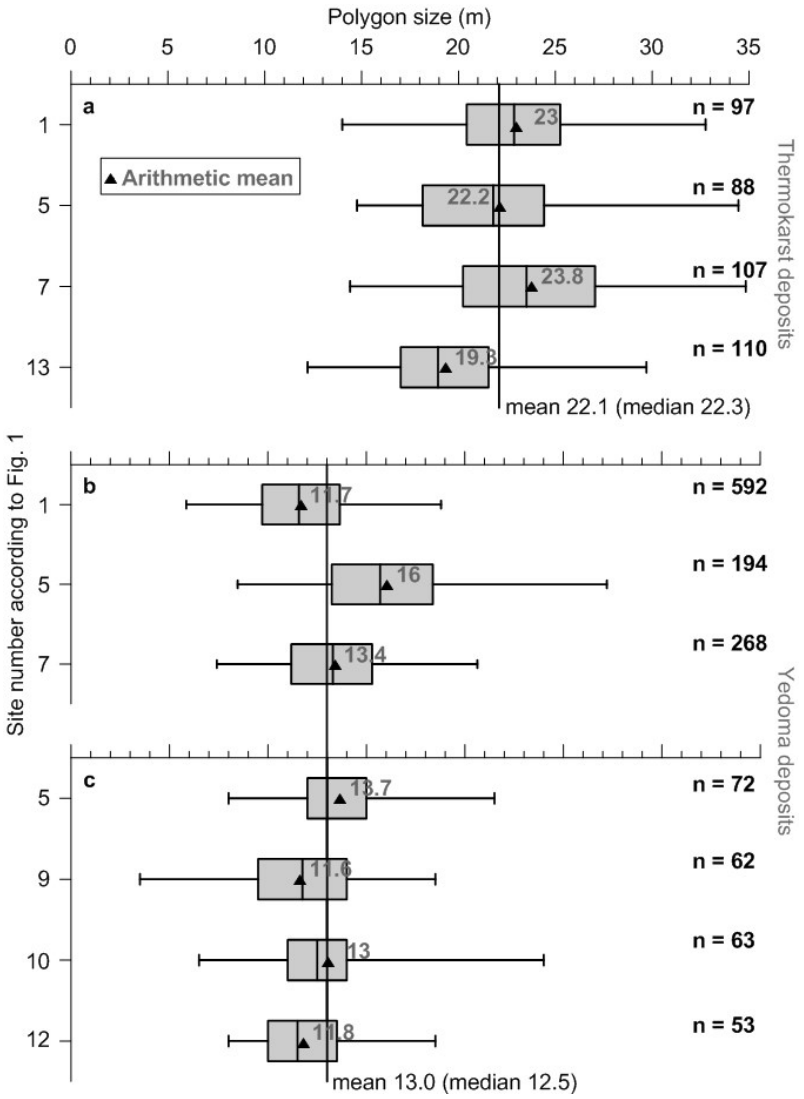

Figure S4. Boxplots of thermokarst (a) and Yedoma (b, c) deposit polygon sizes, including remote-sensing (a and b) and field data (c). The boxplots are numbered according to Fig. 1 (1: Cape Mamontov Klyk; 5: Bykovsky Peninsula; 7: Buor Khaya Peninsula; 9: Bel'kovsky Island; 10: Kotel'ny Island; 12: Maly Lyakhovsky Island; 13: Bol'shoy Lyakhovsky Island). For thermokarst deposits (a), intact surface polygons were mapped (Fig. S3, left side); for Yedoma deposits (b and c), distances between thermokarst mound centers were measured (Fig. S3, right side). Yedoma and thermokarst deposit averages are given by the vertical black line.

Further corroborative evidence for the Yedoma deposit polygon sizes illustrated in Fig. S4 are published by *Tomirdiaro* [1982] and Giterman et al. [1982] for the Siberian lowlands (10-12 m and 9-10 m, respectively) and central Yakutia (11 m) [*Tomirdiaro*, 1982]. Tomirdiaro [1982] describes an average thermokarst deposit polygon size of 20 m (lowlands of northern Yakutia).

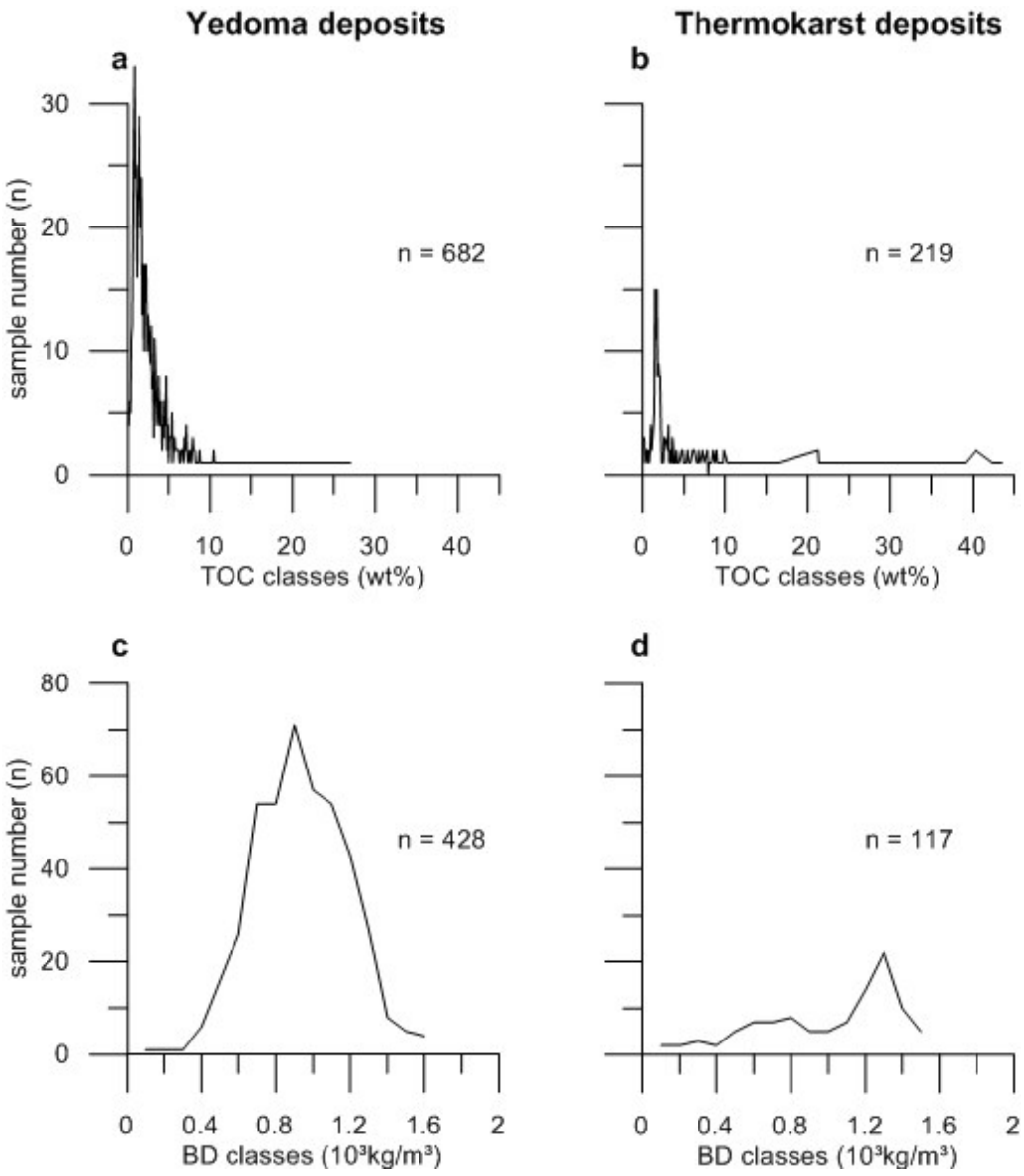

Figure S5. Distribution curves for total organic carbon (TOC, a and b) and bulk density (BD, c and d) to illustrate the non-normal distribution.

3. Supporting Tables

Table S1. . Alternative organic carbon (OC) pool calculations based on simple mean/median. For comparison with previous studies and to illustrate the potential overestimation of the Yedoma region OC pool calculation, the column *"this study (simple mean)"* shows calculations using the arithmetic mean. The column "*this study (simple-median)"* shows an inventory calculation based on median values. [a]Data from *Romanovskii* [1993] and *Jorgenson et al.* [2008], [b]data from *Schirrmeister et al.* [2011], and [c]data from *Kanevskiy et al.* [2011; 2012; 2013] (sites 20, 21 and 23 in Fig. 1) are included. We merged the table cells if just one value is available such as for *Zimov et al.* [2006]; [#] not directly described in the publication, but cited in *Walter et al.* [2007]; *In *Zimov et al.* [2006] the OC density is given as a mean value of ~25.6 kg OC/T, but it is unclear if the WIV is included.

	***Zimov et al.* 2006**	**this study (simple mean)**	**this study (simple-median)**
Yedoma deposits: coverage (km²)	0.50 million	0.41 million[a]	
Thermokarst deposits: coverage (km²)	0.50 million	0.78 million[a]	
Yedoma deposits: thickness (m)	25.0	19.4	15.1
Thermokarst deposits: thickness (m)	½ × Yedoma deposit thickness	5.5	4.6
Yedoma deposits: area affected by degradation (%)	50	70	70
Yedoma deposits: sample number	71	699	
Thermokarst deposits: sample number		224	
Yedoma deposits: BD (10^3kg/m³)	1.65	0.88	0.87
Thermokarst deposits: BD (10^3kg/m³)		0.93	0.98
Yedoma deposits: TOC (wt%)	2.56	3.02[b]	1.89[b]
Thermokarst deposits: TOC (wt%)	70% of Yedoma deposit TOC	6.48[b]	2.59[b]
Yedoma deposits: WIV (vol%)	50	48[c]	52[c]
Thermokarst deposits: WIV (vol%)	n.a.	7	7
Yedoma deposits: SEI (wt%)	n.a.	40.2 [b]	39.8 [b]
Thermokarst deposits: SEI (wt%)	n.a.	40.7[b]	37.5[b]
Yedoma deposits: OC density (kg/m³) WIV included / WIV not considered	25.6*	14 / 27	8 / 16
Thermokarst deposits OC density (kg/m³) WIV included / WIV not considered		56 / 60	24 / 25
Yedoma deposits: OC inventory (Gt)	n.a., 264[#] (~60%)	112 (32%)	50 (37%)
Thermokarst deposits: OC inventory (Gt)	n.a.	240 (68%)	84 (63%)
Total inventory Yedoma region (Gt)	450	352	134

Table S2. Summary of the key parameters for Yedoma deposit organic carbon (OC) budget calculation. [#]Data from *Kanevskiy et al.* [2011; 2012; 2013] (sites 20, 21 and 23 in Fig. 1) are included.

	TOC (wt%)	BD (10^3kg/m^3)	WIV[#] (vol%)	Thickness (m)
Mean	3.02	0.88	47.9	19.4
Median	1.89	0.87	51.9	15.1
16th percentile	0.8	0.63	36.0	9
84th percentile	4.6	1.14	58.4	30
Min	0.1	0.09	34.7	5
Max	27.0	1.52	59.0	46
n	682	428	10	20

Table S3. Summary of the key parameters for thermokarst deposit organic carbon (OC) budget calculation.

	TOC (wt%)	BD (10^3kg/m^3)	WIV (vol%)	Thickness (m)
Mean	6.48	0.93	7.0	5.5
Median	2.59	0.98	6.9	4.6
16th percentile	1.5	0.55	2.6	2
84th percentile	10.4	1.26	12.3	9
Min	0.2	0.09	0.8	1
Max	43.5	1.48	12.8	13
n	219	117	6	10

Table S4. Yedoma deposit parameters separated in a Siberian and an Alaskan subregion.

	TOC (wt%)		BD (10^3kg/m^3)		Thickness (m)	
	Siberia	Alaska	Siberia	Alaska	Siberia	Alaska
Mean	3.20	1.95	0.87	0.95	19.8	18.1
Median	2.03	1.11	0.86	0.94	15.2	15.0
16th percentile	0.9	0.6	0.63	0.67	9	12
84th percentile	4.7	2.9	1.11	1.26	29	25
Min	0.1	0.3	0.09	0.35	5	8
Max	27.0	17.6	1.52	1.40	46	33
n	585	97	351	77	15	5

Table S5. The thermokarst deposit parameters separated in a Siberian and an Alaskan subregion.

	TOC (wt%)		BD (10^3kg/m^3)		Thickness (m)	
	Siberia	Alaska	Siberia	Alaska	Siberia	Alaska
Mean	6.22	9.03	0.94	0.74	6.1	3.1
Median	2.22	7.78	1.05	0.70	4.6	3.1
16th percentile	1.5	3.2	0.55	0.61	2	2
84th percentile	10.0	11.0	1.27	0.76	10	4
Min	0.2	0.5	0.09	0.41	2	1
Max	43.5	42.3	1.48	1.47	13	5
n	199	20	108	9	8	2

Table S6. Polygon size and ice-wedge width used for Yedoma and thermokarst deposit WIV calculation. *Data for wedge-ice width from literature [*Giterman et al.*, 1982; *Meyer et al.*, 2002a,b; *Grigoriev et al.*, 2003; *Magens*, 2005; *Boike et al.*, 2008; *Wetterich et al.*, 2008; *Hoffmann*, 2011; *Kanevskiy et al.*, 2011, 2012, 2013; *Opel et al.*, 2011; *Boereboom et al.*, 2013] and field measurements.

	Yedoma deposit ice-wedge width (m)*	Yedoma deposit polygon size (m)	Thermokarst deposit ice-wedge width (m)*	Thermokarst deposit polygon size (m)
mean	4.0	13.0	1.7	22.1
median	4.2	12.5	1.6	22.3
16th percentile	2.6	11.6	0.6	20.3
84th percentile	4.5	13.4	2.9	23.2
min	2.4	3.5	0.2	12.2
max	6.0	27.2	3.0	34.8
number of sites	10	7	6	4
n total	44	1,304	40	402

Table S7. Existing data on thermokarst affected areas and lakes in the Yedoma region. *excluding slope areas; **only thaw lake basins without slopes or thermoerosional forms; ***area covered by 11 digitized maps, including areas outside the Yedoma region.

Reference	Region	Study area (km²)	Thermokarst-affected area (km²)	Thermokarst affected area (%)	Yedoma deposit area (km²)	Yedoma deposit area (%)	Lake area (%)
Grosse et al. [2005]*	Bykovsky Peninsula, Siberia	175	93	53	n.a.	n.a.	14.4
Grosse et al. [2006]	Cape Mamontov Klyk, Siberia	2,317	1,807	78	515	22	8.9
Veremeeva and Gubin [2009]	Kolyma Lowland, Siberia	6,528	4,231	65	1,730	27	18
Morgenstern et al. [2011]**	Lena Delta, Siberia	1,689	338	20	n.a.	n.a.	7.0
Morgenstern et al. [2011]	Kurungnakh Island, Siberia	259	172	66	87.4	34	
Arcos [2012]	Buor Khaya Peninsula, Siberia	2,000	1,800	90	200	10	8.8
Jones et al. [2012]	northern Seward Peninsula, Alaska	515	391	76	n.a.	n.a.	7
Grosse et al. [2013b] ***	northern Siberia	1,716,946	n.a.	n.a.	290,101	17	n.a.

Table S8. Sensitivity analyses for "mean-based" bootstrapping methods for the four variables for which multiple observations were available. Results were obtained when the uncertainty around a single variable was set to zero (fixed); they were presented as the % of the range obtained from the original run. For comparison, the results of mean, range from the mean to the 16th, and 84th percentiles and 84th-16th absolute percentile range are indicated.

	mean (Gt)	range to 16th per-centile (Gt)	range to 84th per-centile (Gt)	per-centile range (Gt)	TOC fixed (%)	BD fixed (%)	WIV fixed (%)	thickness fixed (%)
Yedoma	111	95	128	33	96	98	93	50
Thermokarst	237	181	294	113	93	100	100	35

Table S9. Yedoma region organic carbon pool calculated with arithmetic means and standard (std) deviation estimates

	Yedoma			Thermokarst		
	mean	Std deviation	Std error	mean	Std deviation	Std error
TOC (wt%)	3.0	3.6	0.14	6.5	8.9	0.60
BD (10^3kg/m^3)	0.9	0.2	0.01	0.9	0.4	0.03
(100-WIV)/100	0.5	0.07	0.02	0.9	0.05	0.02
Thickness (m)	19.4	11.5	2.63	5.5	4.0	1.25
OC budget (Gt)	112			240		
± Propagation error	17			60		

Supporting References

Arcos, D. R. (2012), Classification of Periglacial Landforms Based on High Resolution Multispectral Remote Sensing Data. A Contribution to the Landscape Description of the North Siberian Buor Khaya Pensinsula, diploma thesis, 71 pp, Potsdam University, Potsdam.

Battle, M., M. L. Bender, P. P. Tans, J. W. C. White, J. T. Ellis, T. Conway, and R. J. Francey (2000), Global carbon sinks and their variability inferred from atmospheric O_2 and $\delta^{13}C$, *Science*, *287*(5462), 2467-2470, doi: 10.1126/science.287.5462.2467.

Boereboom, T., D. Samyn, H. Meyer, and J. L. Tison (2013), Stable isotope and gas properties of two climatically contrasting (Pleistocene and Holocene) ice wedges from Cape Mamontov Klyk, Laptev Sea, northern Siberia, *The Cryosphere*, *7*(1), 31-46, doi: 10.5194/tc-7-31-2013.

Boike, J., D. Y. Bolshiyanov, L. Schirrmeister, and S. Wetterich (2008), *Reports on Polar and Marine Research - Russian-German Cooperation SYSTEM LAPTEV SEA: The Expedition Lena - New Siberian Islands 2007 during the International Polar Year 2007/2008*, 265 pp., Alfred Wegener Institute for Polar and Marine Research, Bremerhaven.

Giterman, R. E., A. V. Sher, and J. V. Matthews (1982), Comparison of the Development of Tundra-Steppe Environments in West and East Beringia: Pollen and Macrofossil Evidence from Key Sections, in *Paleoecology of Beringia*, edited by D. M. Hopkins, J. V. Matthews, C. E. Schweger and S. B. Young, pp. 43-73, Academic Press, New York.

Grigoriev, M. N., V. Rachold, D. Y. Bolshiyanov, E.-M. Pfeiffer, L. Schirrmeister, D. Wagner, and H.-W. Hubberten (2003), *Reports on Polar and Marine Research - Russian-German Cooperation SYSTEM LAPTEV SEA - The Expedition LENA 2002*, 341 pp., Alfred Wegener Institute for Polar and Marine Research, Bremerhaven.

Grosse, G., L. Schirrmeister, and T. J. Malthus (2006), Application of Landsat-7 satellite data and a DEM for the quantification of thermokarst-affected terrain types in the periglacial Lena-Anabar coastal lowland, *Polar Res.*, *25*(1), 51-67, doi: 10.1111/j.1751-8369.2006.tb00150.x.

Grosse, G., B. Jones, and C. D. Arp (2013a), Thermokarst Lakes, Drainage, and Drained Basins, in *Treatise in Geomorphology*, edited by J. F. Shroder, pp. 325-353, Academic Press, San Diego.

Grosse, G., L. Schirrmeister, V. V. Kunitsky, and H.-W. Hubberten (2005), The use of CORONA images in remote sensing of periglacial geomorphology: An illustration from the NE Siberian Coast, *Perm. Periglac. Process.*, *16*(2), 163-172, doi: 10.1002/ppp.509.

Grosse, G., V. E. Romanovsky, K. M. Walter, A. Morgenstern, H. Lantuit, and S. Zimov (2008), Distribution of thermokarst lakes and ponds at three Yedoma sites in Siberia, *Proceedings of the Ninth International Conference on Permafrost*, *1*, 551-556.

Grosse, G., J. E. Robinson, R. Bryant, M. D. Taylor, W. Harper, A. DeMasi, E. Kyker-Snowman, A. Veremeeva, L. Schirrmeister, and J. Harden (2013b), Distribution of late Pleistocene ice-rich syngenetic permafrost of the Yedoma Suite in east and central Siberia, Russia, *U.S.G.S. Open File Report*, *1078*, 37.

Hoffmann, K. (2011), Holocene Climate Variability of the Central Lena Delta, Northern Siberia – Implications from Ground Ice, master thesis, 148 pp, University of Bonn, Bonn.

Jones, M. C., G. Grosse, B. M. Jones, and K. M. Walter Anthony (2012), Peat accumulation in drained thermokarst lake basins in continuous, ice-rich permafrost, northern Seward Peninsula, Alaska, *J. Geophys. Res.*, *117*, G00M07, doi: 10.1029/2011JG001766.

Jorgenson, M. T., K. Yoshikawa, M. Kanveskiy, Y. Shur, V. Romanovsky, S. Marchenko, G. Grosse, J. Brown, and B. Jones (2008), Permafrost characteristics of Alaska, *Proceedings of the Ninth International Conference on Permafrost*, *3*, 121–122.

Kanevskiy, M., Y. Shur, D. Fortier, M. T. Jorgenson, and E. Stephani (2011), Cryostratigraphy of late Pleistocene syngenetic permafrost (yedoma) in northern Alaska, Itkillik River exposure, *Quat. Res.*, *75*(3), 584-596, doi: 10.1016/j.yqres.2010.12.003.

Kanevskiy, M., Y. Shur, B. Connor, M. Dillon, E. Stephani, and J. O'Donnell (2012), Study of the ice-rich syngenetic permafrost for road design (Interior Alaska), *Proceedings of the Tenth International Conference on Permafrost*, *1*, 191-196.

Kanevskiy, M., Y. Shur, M. T. Jorgenson, C. L. Ping, G. J. Michaelson, D. Fortier, E. Stephani, M. Dillon, and V. Tumskoy (2013), Ground ice in the upper permafrost of the Beaufort Sea coast of Alaska, *Cold Reg. Sci. Technol.*, *85*, 56-70, doi: 10.1016/j.coldregions.2012.08.002.

Magens, D. (2005), Late Quaternary Climate and Environmental History of the Siberian Arctic - Permafrost Records from Cape Mamontovy Klyk, Laptev Sea, master thesis, 131 pp, Christian-Albrechts-University Kiel, Kiel.

Meyer, H., A. Dereviagin, C. Siegert, and H. W. Hubberten (2002a), Paleoclimate studies on Bykovsky Peninsula, North Siberia - Hydrogen and oxygen isotopes in ground ice, *Polarforschung*, *70*(1/2), 37–51, doi: 10.1594/PANGAEA.728530.

Meyer, H., A. Dereviagin, C. Siegert, L. Schirrmeister, and H.-W. Hubberten (2002b), Palaeoclimate reconstruction on Big Lyakhovsky Island, north Siberia - Hydrogen and oxygen isotopes in ice wedges, *Perm. Periglac. Process.*, *13*(2), 91-105, doi: 10.1002/ppp.416.

Morgenstern, A. (2012), Thermokarst and Thermal Erosion: Degradation of Siberian Ice-Rich permafrost, PhD thesis, 116 pp, Potsdam University, Potsdam.

Morgenstern, A., G. Grosse, F. Günther, I. Fedorova, and L. Schirrmeister (2011), Spatial analyses of thermokarst lakes and basins in Yedoma landscapes of the Lena Delta, *The Cryosphere*, *5*(4), 849-867, doi: 10.5194/tc-5-849-2011.

Opel, T., A. Y. Dereviagin, H. Meyer, L. Schirrmeister, and S. Wetterich (2011), Palaeoclimatic information from stable water isotopes of Holocene ice wedges on the Dmitrii Laptev Strait, northeast Siberia, Russia, *Perm. Periglac. Process.*, *22*(1), 84-100, doi: 10.1002/ppp.667.

Romanovskii, N. N. (1993), *Fundamentals of Cryogenesis of Lithosphere*, 336 pp., Moscow University Press, Moscow.

Schirrmeister, L., D. G. Froese, V. Tumskoy, G. Grosse, and S. Wetterich (2013), Yedoma: Late Pleistocene Ice-Rich Syngenetic Permafrost of Beringia, in *Encyclopedia of Quaternary Sciences*, edited by S. A. Elias, Elsevier, Amsterdam.

Schirrmeister, L., G. Grosse, S. Wetterich, P. P. Overduin, J. Strauss, E. A. G. Schuur, and H.-W. Hubberten (2011), Fossil organic matter characteristics in permafrost deposits of the northeast Siberian Arctic, *J. Geophys. Res.*, *116*, G00M02, doi: 10.1029/2011jg001647.

Strauss, J., L. Schirrmeister, S. Wetterich, A. Borchers, and S. P. Davydov (2012), Grain-size properties and organic-carbon stock of Yedoma Ice Complex permafrost from the Kolyma lowland, northeastern Siberia, *Glob. Biogeochem. Cycles*, *26*(3), GB3003, doi: 10.1029/2011GB004104.

Tomirdiaro, S. V. (1982), Evolution of Lowland Landscapes in Northeastern Asia during Late Quaternary Time, in *Paleoecology of Beringia*, edited by D. M. Hopkins, J. V. Matthews, C. E. Schweger and S. B. Young, pp. 29-37, Academic Press, New York.

Ulrich, M., E. Hauber, U. Herzschuh, S. Härtel, and L. Schirrmeister (2011), Polygon pattern geomorphometry on Svalbard (Norway) and western Utopia Planitia (Mars) using high-resolution stereo remote-sensing data, *Geomorphol.*, *134*(3–4), 197-216, doi: 10.1016/j.geomorph.2011.07.002.

van Everdingen, R. O. (1998, revised 2005), *Multi-Language Glossary of Permafrost and Related Ground-Ice Terms*, 233 pp. pp., National Snow and Ice Data Center, Boulder, CO, USA.

Veremeeva, A., and S. V. Gubin (2009), Modern tundra landscapes of the Kolyma Lowland and their evolution in the Holocene, *Perm. Periglac. Process.*, *20*(4), 399-406, doi: 10.1002/ppp.674.

Walker, H. J. (1998), Arctic deltas, *J. Coast. Res.*, *14*(3), 718-738.

Walter, K. M., L. C. Smith, and S. F. Chapin (2007), Methane bubbling from northern lakes: present and future contributions to the global methane budget, *Philos. Trans. Roy. Soc. London Ser. A*, *365*(1856), 1657-1676, doi: 10.1098/rsta.2007.2036.

Wetterich, S., S. Kuzmina, A. Andreev, F. Kienast, H. Meyer, L. Schirrmeister, T. Kuznetsova, and M. Sierralta (2008), Palaeoenvironmental dynamics inferred from late Quaternary permafrost deposits on Kurungnakh Island, Lena Delta, Northeast Siberia, Russia, *Quat. Sci. Rev.*, *27*(15–16), 1523-1540, doi: 10.1016/j.quascirev.2008.04.007.

Zimov, S. A., S. P. Davydov, G. M. Zimova, A. I. Davydova, E. A. G. Schuur, K. Dutta, and F. S. Chapin (2006), Permafrost carbon: Stock and decomposability of a globally significant carbon pool, *Geophys. Res. Lett.*, *33*(20), L20502, doi: 10.1029/2006GL027484